Lithos 134-135 (2012) 221–235

Contents lists available at SciVerse ScienceDirect

Lithos

journal homepage: www.elsevier.com/locate/lithos

Stabilization of garnet in metamorphosed altered turbidites near the St. Eugene lead–zinc deposit, southeastern British Columbia: Equilibrium and kinetic controls

David R.M. Pattison *, JennaLee D. Seitz

Department of Geoscience, University of Calgary, 2500 University Drive N.W., Calgary, Alberta, Canada T2N 1N4

ARTICLE INFO

Article history:
Received 19 June 2011
Accepted 17 December 2011
Available online 26 December 2011

Keywords:
Hydrothermal alteration
Metamorphism
Garnet
Thermodynamic modeling
Kinetics
Vectors to mineralization

ABSTRACT

The St. Eugene lead-zinc deposit, near Moyie, southeastern British Columbia, is a Mesoproterozoic vein deposit hosted by metaturbidites of the 1.5–1.4 Ga Belt–Purcell Supergroup. The regional metamorphic grade of the rocks is biotite zone, with the age of metamorphism being Mesoproterozoic (ca. 1.35 Ga). The vein system is enveloped by a metamorphosed alteration zone of increasing intensity as the vein is approached. Thin argillaceous tops of turbidite beds away from the vein are garnet-free, whereas those in the inner alteration zone are garnet-bearing. Compared to rocks away from the vein, those near the vein are enriched in Fe, Mn, Pb and Zn, with proportional reduction in other compositional parameters. Thermodynamic modeling of three rocks across the alteration gradient predicts increasing stabilization of garnet with increasing degree of alteration. Predicted and observed modes of garnet in the samples are in close agreement. In the most altered rock, the garnet-in line is displaced down-temperature by ~100 °C relative to the least altered rock. Approximately 2/3 of the garnet stabilization is accounted for by increase in Mn content and the rest by increase in Fe/(Fe + Mg). Kinetic factors played a role in the development of the mineral assemblages, including metastable persistence of zoisite, and disequilibrium (overstepped) initial growth of garnet. Estimates of peak pressure–temperature conditions from mineral assemblage constraints and from compositional isopleths are complicated by the kinetic effects but yield similar results: 490–510 °C and 3.6–4.0 kbar. The pressure–temperature estimates imply an average linear geothermal gradient of ~35 °C/km, broadly consistent with burial metamorphism in the Belt–Purcell extensional basin. However, the estimated pressure, equivalent to a depth of 13–15 km, is greater than the estimated ~8 km (~2.2 kbar) of stratigraphic overburden at the time of metamorphism. The results of this study support the idea that garnet is a useful indicator mineral ('vector') for hydrothermal alteration associated with base and precious metal mineralization in this region, and potentially in other regions of comparable metamorphic grade. The ideal metamorphic conditions under which garnet is useful in this role are the metapelitic chlorite and biotite zones (greenschist and lower amphibolite facies).

1. Introduction

The purpose of this paper is to describe the petrology of an exceptional natural locality that illustrates the stabilizing effects of Mn and Fe on garnet in metapelites. The locality comprises metamorphosed altered turbidites in the vicinity of the St. Eugene lead–zinc vein system in the Omineca Belt of the Canadian Cordillera, in southeastern British Columbia (Fig. 1). This study provides a natural complement to experimental and theoretical treatments of the stabilizing effect of Fe and Mn on garnet (e.g., Atherton, 1977; Loomis, 1986; Spear, 1988; Spear & Cheney, 1989; Symmes & Ferry, 1992; Droop & Harte, 1995; Mahar et al., 1997; Tinkham et al., 2001; Wei et al., 2004; Caddick and Thompson, 2008). The above studies calculated that the stability of garnet could be displaced down-temperature by as much as 100 °C in rocks high in Fe/(Fe + Mg) and especially Mn relative to metapelites of average composition (e.g., Shaw, 1956).

A secondary aim of the paper is to estimate pressure–temperature (P–T) conditions of garnet formation at St. Eugene. P–T estimates are made by comparing the observed mineral assemblages and compositions with predictions from phase equilibrium modeling. Our analysis suggests that disequilibrium processes played a role in the development of the garnet-bearing mineral assemblages, in particular reaction overstepping and metastable persistence of the porphyroblastic reactant mineral zoisite. This study therefore continues a trend in which the role of disequilibrium processes in contact and regional metamorphism is increasingly recognized (e.g., Chernoff and Carlson, 1997; Waters and Lovegrove, 2002; Carlson, 2002; Zeh and Holness, 2003; Pattison et al., 2011, and references therein). In addition to being of petrological interest, this study bears on two regional geological issues: the significance of isolated occurrences of garnet-bearing rocks in the Purcell Anticlinorium of the Omineca Belt (thermal anomalies vs. unusual rock compositions); and the potential

* Corresponding author. Fax: +1 403 284 0074.
E-mail address: pattison@ucalgary.ca (D.R.M. Pattison).

0024-4937/$ – see front matter © 2011 Published by Elsevier B.V.
doi:10.1016/j.lithos.2011.12.007

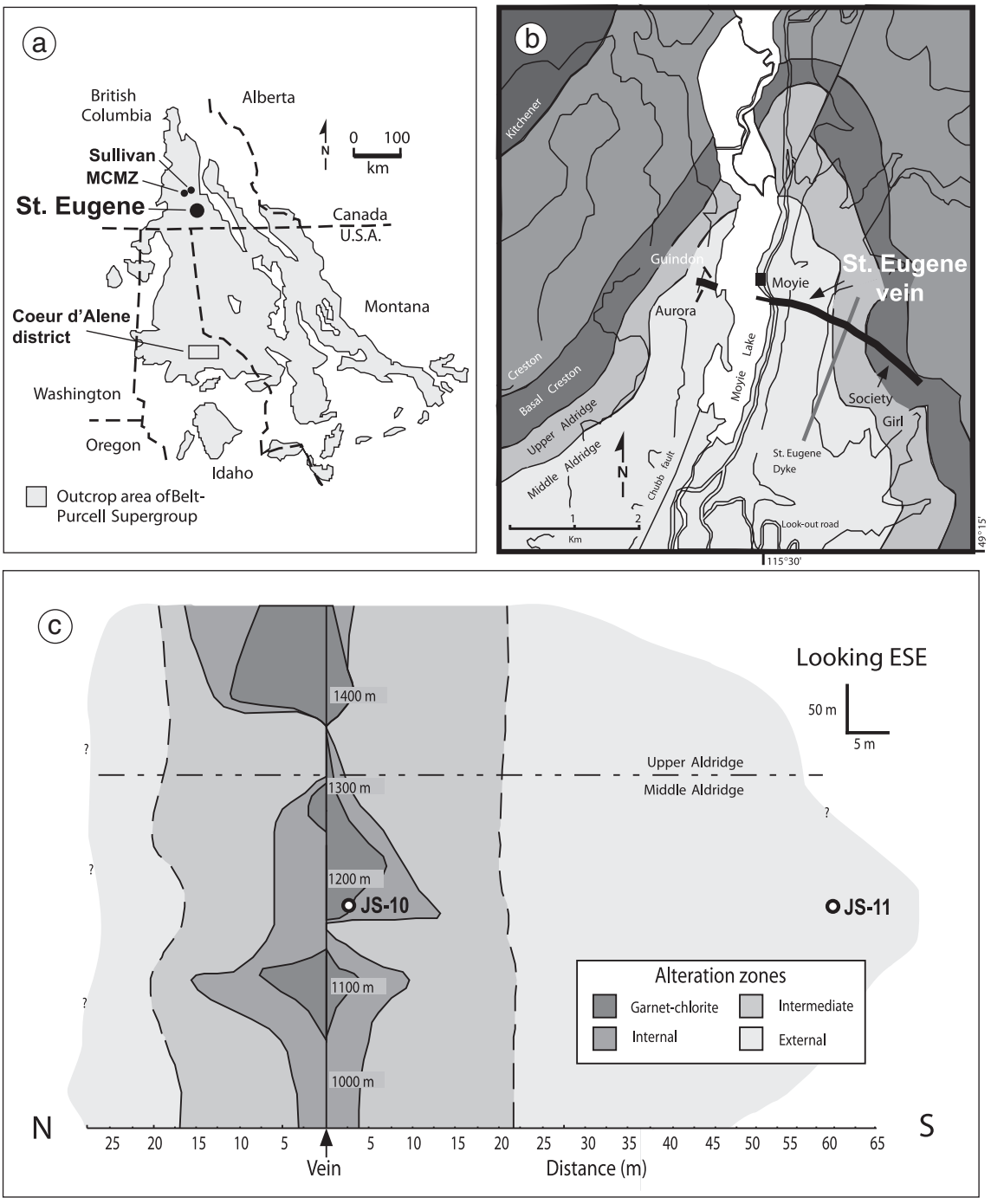

Fig. 1. (a) Areal extent of Belt–Purcell rocks in southeastern British Columbia, southwestern Alberta, northwestern Montana, northern Idaho and northeastern Washington, and location of St. Eugene, Sullivan and Matthew Creek areas (figure modified from Joncas and Beaudoin, 2002). (b) Geology of the area in the vicinity of the St. Eugene vein system (after Hoy, 1993). The vein system is located near the crest of the Moyie anticline and transects the Middle Aldridge Formation, Upper Aldridge Formation and lower parts of the Creston formations of the Belt–Purcell Supergroup. (c) Vertical NNE cross-section, looking ESE, of the St. Eugene vein system showing the surrounding alteration zones defined by Joncas and Beaudoin (2002). Location of samples JS-10 and JS-11 indicated.

utility of garnet as an indicator mineral ('vector') to ore mineralization (cf. Joncas and Beaudoin, 2002).

2. Regional geological setting

2.1. Stratigraphy

The St. Eugene vein system is hosted in broadly folded quartzites, wackes and argillites of the Middle and Upper Aldridge Formations and the basal part of the Creston Formation of the Mesoproterozoic (ca. 1.5–1.4 Ga) Belt–Purcell Supergroup (Hoy et al., 2000; Fig. 1a and b). The Belt–Purcell Supergroup represents infilling of an intracontinental rift system developed within the once-contiguous North American and Australian or Siberian cratons (see discussion in Lydon, 2000, 2007), the latter subsequently rifted away from the western margin of the North American craton in the Eocambrian with the opening of the proto-Pacific Ocean. The Aldridge Formation represents the 'rift-fill' facies of the Belt–Purcell Supergroup, whereas the Creston Formation marks the transition into the 'rift cover' facies (Hoy et al., 2000). Estimates of maximum thickness of the Belt–

Purcell Supergroup are in the range 15–20 km (Hoy, 1993; Hoy et al., 2000), 10–12 km of which are estimated to occur above the Middle-Lower Aldridge boundary (Hoy, 1993; Hoy et al., 2000). Abundant tholeiitic mafic sills dated at 1468 Ma (Anderson and Davis, 1995), known as the Moyie Sills, were emplaced into wet, turbiditic sediments of the Aldridge Formation (Hoy, 1989). Mafic magmatism continued for at least another 100 Ma in the region (see compilations in Lydon, 2000, 2007). The Belt–Purcell strata are unconformably overlain by strata of the Neoproterozic Windermere Supergroup, another intracratonic rift-related sedimentary package, and in turn by Cambrian and younger strata of the passive margin sequence (miogeocline) that developed on the rifted North American margin of the proto-Pacific Ocean.

2.2. Structure

The St. Eugene vein system occurs near the crest of the Moyie Anticline (Fig. 1b), a broad fold on the east flank of the Purcell Anticlinorium. The Purcell Anticlinorium is the dominant regional structure of the eastern part of the Omineca Belt of the southern Canadian Cordillera. It is a broad, north-trending, gently north-plunging structural culmination cored by rocks of the Belt–Purcell Supergroup. The trend of the Purcell Anticlinorium is shown approximately in Fig. 1a by the tongue of Belt–Purcell rocks that extends north from the Canada–USA border into British Columbia. The Purcell Anticlinorium and Moyie Anticline are Mesozoic structures. They formed during contractional orogenesis in the Jurassic–Paleocene that gave rise to the southern Canadian Cordillera. Price and Sears (2000) estimated that the sedimentary rocks of the Purcell Anticlinorium were tectonically transported ~200 km eastwards from where they were deposited.

In the Belt–Purcell rocks, mesoscale structural features associated with the Cordilleran folding and faulting are variably developed. They include locally developed crenulations and spaced cleavage (McMechan and Price, 1982; McFarlane and Pattison, 2000; Turner et al., 2000). These fabrics overprint earlier, also variably developed, fabrics that generally increase in intensity with stratigraphic depth in the Belt–Purcell stratigraphy (McMechan and Price, 1982; Hoy, 1993). These earlier fabrics range from a weak foliation parallel to bedding in argillaceous layers at higher stratigraphic levels, to a more penetrative cleavage at moderate to high angles to bedding that is most pronounced in the lowest stratigraphic levels, such as the Lower Aldridge Formation (Leech, 1962; McMechan and Price, 1982; Hoy, 1993; McFarlane and Pattison, 2000). The weak foliation parallel to bedding may reflect burial-related alignment of sheet silicates, accentuated by metamorphic recrystallization. The transecting fabrics have been ascribed by Leech (1962) and McMechan and Price (1982) to Proterozoic deformation, based on their absence in the overlying Windermere and younger sediments and the observation that the ca. 1365 Ma Hellroaring Creek Stock cuts a transecting foliation in the host Aldridge metasediments. There are few demonstrable Proterozoic fold structures with which the transecting microfabrics are developed, a feature ascribed by Reesor (in Leech, 1962, p. 5) to similar trends of the Proterozoic and later, more dominant, overprinting, Mesozoic structures.

2.3. Metamorphism

The ambient metamorphic grade of the large tract of rocks belonging to the lower part of the Belt–Purcell Supergroup (Aldridge Formation) in the core of the southern Purcell Anticlinorium is of the epidote amphibolite facies (sometimes termed lower amphibolite facies or transitional greenschist-amphibolite facies). This assignment is based on the widespread occurrence of metamorphic hornblende with combinations of actinolitic amphibole, epidote, chlorite, plagioclase, calcite, quartz and titanite in the Moyie Sills (Brown and Stinson, 1995; Anderson and Goodfellow, 2000; Schandl and Davis, 2000; McFarlane and Pattison, 2000; Pattison et al., 2010). This assignment differs from earlier works stating that the regional metamorphic grade is of the greenschist facies (e.g., Leech, 1962; McMechan and Price, 1982; Greenwood et al., 1991; Read et al., 1991).

Argillaceous rocks of the Aldridge Formation that host the hornblende-bearing Moyie Sills largely belong to the regional biotite zone, based on the widespread occurrence of muscovite + biotite ± chlorite-bearing mineral assemblages (McMechan and Price, 1982; Read et al., 1991; Brown and Stinson, 1995; Pattison et al., 2010). This implies, contrary to convention, that the lower limit of amphibolite facies metamorphism occurs within the metapelitic biotite zone rather than the metapelitic garnet zone. Other regions in southeastern British Columbia where epidote amphibolite facies metabasic rocks are interbedded with biotite zone argillaceous rocks include the region between Salmo and Nelson (Powell and Ghent, 1996; Pattison et al., 2010), and the domain north of the town of Granby (Laberge and Pattison, 2007).

At higher stratigraphic levels of the Belt–Purcell Supergroup, approximately above the Aldridge Formation, the grade is predominantly of the metapelitic chlorite zone (McMechan and Price, 1982), corresponding to the greenschist facies. The overall pattern of increasing degree of metamorphism with stratigraphic depth in the Belt–Purcell Supergroup has led to the suggestion that the metamorphism of the Belt–Purcell rocks is broadly of burial type (Greenwood et al., 1991; McMechan and Price, 1982), an interpretation that is consistent with the widespread, regional development (1000's km^2) of the biotite zone in the lower levels of the Belt–Purcell Supergroup in the southern Purcell Anticlinorium. Contrasts in fabric intensity and metamorphic grade across the unconformity between the Belt–Purcell strata and overlying NeoProterozoic Windermere strata (e.g., from biotite to chlorite zones in the St. Mary River area; Leech, 1967) provide evidence for metamorphism and deformation of the Belt–Purcell rocks prior to NeoProterozoic uplift, erosion and Windermere sedimentation.

2.4. Garnet-bearing rocks

Pockets of garnet-bearing rocks occur in a few localities in the Purcell Anticlinorium, most of which are hosted in the Aldridge Formation. The garnet-bearing rocks can be divided into three types. The first type occurs in the Matthew Creek Metamorphic Zone, located 5 km SW of Kimberley, BC (MCMZ; McFarlane and Pattison, 2000; Pattison et al., 2010; Fig. 1a). The MCMZ is an anomalous, ~5 × 8 km^2, ductile fault-bounded domain of high metamorphic grade (middle-upper amphibolite facies) characterized by glistening, lineated muscovite–biotite–garnet–sillimanite ± andalusite ± staurolite schists belonging to the Lower Aldridge Formation. In contrast, rocks of the Lower Aldridge Formation overlying and surrounding the MCMZ are typical of the regionally extensive biotite zone. The peak metamorphic conditions at Matthew Creek were 3.5–4.0 kbar and 600–650 °C (McFarlane and Pattison, 2000; Pattison et al., 2010). The MCMZ thus represents a local, fault-bounded thermal anomaly in the lowest part of the Belt–Purcell rift basin, most likely related to Mesoproterozoic mafic magmatism (see below).

The second type of garnet-bearing rocks comprises rocks of unusual composition, spatially associated with syngenetic or epigenetic hydrothermal mineralization, within regions of ambient biotite zone metamorphic conditions. Examples include: St. Eugene (Joncas and Beaudoin, 2002; this study); the Sullivan Mine and related deposits in the 'Sullivan-North Star corridor' (DePaoli and Pattison, 1995, 2000; Slack et al., 2000; Turner et al., 2000); the Fors deposit, located 10 km NNE of St. Eugene (Britton and Pighin, 1995); and the Mount Mahon area, located ~27 km SSW of St. Eugene (Brown and Stinson, 1995; Brown, 1998) (see Fig. 1a). Examples of the second type in

the USA include the Hercules, Frisco and Success deposits of the Coeur d'Alene district of Idaho (Frycklund, 1964) (Fig. 1a).

The peak metamorphic conditions at Sullivan were estimated to be 3.8 ± 1.0 kbar and 450 ± 50 °C (DePaoli and Pattison, 1995, 2000), i.e. of lower temperature but similar pressure to the nearby sillimanite ± andalusite schists of the MCMZ. The garnet in the Sullivan rocks is manganese-rich (Mn/(Mn + Fe + Mg + Ca) = ~0.1–0.8, De Paoli and Pattison, 1995, 2000; Jiang et al., 1998; Slack et al., 2000), most likely accounting for its presence in rocks belonging to the regional biotite zone (e.g., Mahar et al., 1997; Spear and Cheney, 1989; Tinkham et al., 2001; Caddick and Thompsion, 2008). Based on an average rock density of 2.7 g/cm^3, corresponding to a mixture of siliciclastic metasediments and sparser carbonate and amphibolite layers, 3.8 kbar represents a depth of ~14 km, close to the stratigraphic estimate of 10–12 km of Belt–Purcell sediments above the Lower–Middle Aldridge transition where the Sullivan ore body is located (Hoy, 1993; Lydon, 2000). Combining the 10–14 km depth range with the 450 °C temperature estimate yields an average (linear) geothermal gradient of 32–45 °C/km. Such a geothermal gradient is consistent with the location of the ore body in a rift-basin setting accompanied by mafic magmatism that outlasted sedimentation (Lydon, 2000).

The third variety of garnet-bearing rocks comprises localities in which garnet has been reported but not studied in detail. These localities include Middle Aldridge rocks north and west of St. Mary Lake, approximately 10 km WNW of the MCMZ, where garnet occurs with

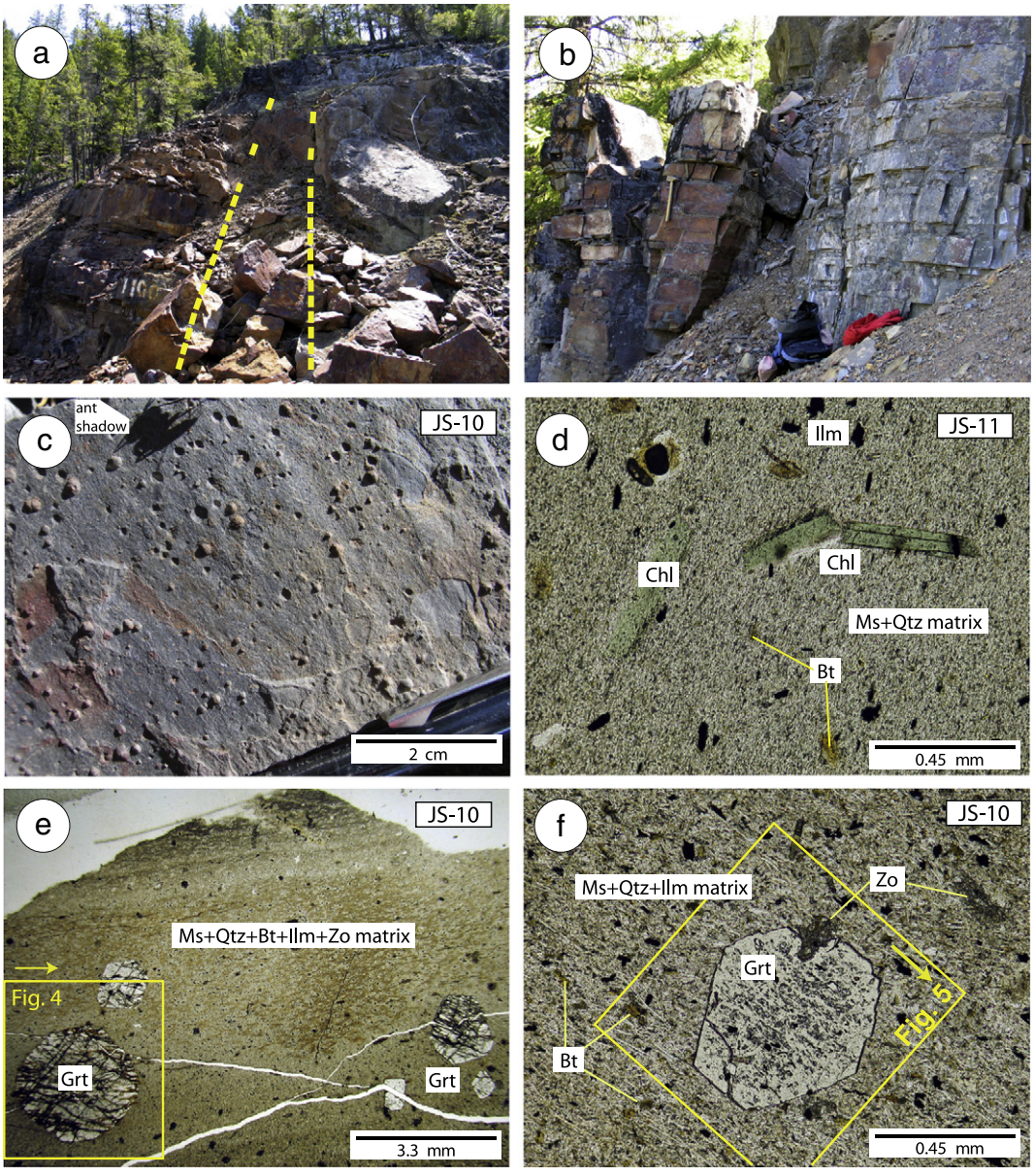

Fig. 2. (a) Photograph of the outcrop expression of the St. Eugene vein system at the 1100 level, ~1170 m elevation. At the surface the vein system comprises a narrow, subvertical, rusty, sulfide-bearing domain (approximately within the yellow dashed lines) that transects the gently dipping metaturbidites of the Middle Aldridge Formation. The vein thickens with depth. (b) Typical gently dipping metaturbidites of the Middle Aldridge Formation within 60 m of the vein system, showing thicker, light-colored, quartz-rich sandstone layers and thinner, dark-colored, argillaceous layers. The thin argillaceous layers are the focus of the study. (c) Sample JS-10, collected < 10 m from the vein system. Argillaceous bedding surface with abundant garnets. (d) Sample JS-11, collected from regional country rocks ~60 m from the vein system. Chlorite and biotite porphyroblasts occur in a fine grained muscovite ± chlorite + ilmenite + quartz matrix. Zoisite (not visible in photomicrograph) is variably present. (e) Sample JS-10. Garnets of various sizes in a fine grained argillaceous matrix showing bedding. The location of Fig. 4 (compositional X-ray maps of garnet) is shown in the yellow box, with the arrow pointing to the top of the images in Fig. 4. (f) Sample JS-10. The garnet has overgrown a weak planar matrix fabric parallel to bedding. The location of Fig. 5 (compositional X-ray maps of garnet) is shown in the yellow box, with the arrow pointing to the top of the images in Fig. 5. (For interpretation of the references to color in this figure legend, the reader is referred to the web version of this article.)

combinations of chlorite, biotite, epidote and reportedly andalusite in argillaceous layers (Berry, 1951), and Upper Aldridge rocks located 20 km south of St. Eugene and ~3 km SW of Mt. Olson, where garnet occurs with amphibole in laminated siltstones (Leech, 1967).

2.5. Age of metamorphism and relation to orogenic events

Despite the Purcell Anticlinorium being a major Cordilleran (Mesozoic) structure, the age of the regional biotite-zone metamorphism of the Belt–Purcell rocks in its core is Mesoproterozoic. Arguments in support of this conclusion are summarized in McMechan and Price (1982). The primary evidence is the widespread occurrence of Proterozoic (700–1330 Ma) K–Ar cooling ages from metamorphic biotite contained in a variety of rocks, including: argillites from the Aldridge Formation and correlative Prichard Formation in Idaho; basaltic sills ('Moyie sills') emplaced in the Aldridge Formation; metamorphosed alteration zones associated with mineralization at St. Eugene; and Proterozoic granitoid intrusions (Hoy, 1993; Leech, 1967; Obradovich and Peterman, 1968).

Several U–Pb dates in the region indicate that a Mesoproterozoic metamorphic event affected the Belt–Purcell rocks. Metamorphic titanite from altered rocks of the Sullivan ore body, and from a Moyie Sill south of the orebody, fall in the range 1320–1350 Ma (Ross et al., 1992; Schandl et al., 1993; Schandl & Davis, 2000). Metamorphic monazite from schists of the Matthew Creek Metamorphic Zone fall in the range 1340–1350 Ma (Anderson and Davis, 1995; Anderson and Parrish, 2000), with more recent dating yielding some ages around 1410 Ma (C.R.M. McFarlane and M.W. Williams, unpublished data, 2011). Igneous zircon from muscovite + garnet + tourmaline-bearing (S-type) pegmatitic trondjhemitic intrusions of the Hellroaring Creek suite, located 5 km SW of the MCMZ and mineralogically the same as small pegmatitic sills in the MCMZ, were dated at ca. 1365 Ma (J. Mortensen, unpublished data; Anderson and Parrish, 2000). In the Salmon River Arch in Idaho, high grade metamorphism was dated at ca. 1370 Ma by Doughty and Chamberlain (1996).

This episode of Mesoproterozoic regional metamorphism has been termed the East Kootenay Orogeny (White, 1959; Leech, 1962; McMechan and Price, 1982; Anderson and Parrish, 2000; Lydon, 2000). The East Kootenay Orogeny appears to record a period of renewed extension, mafic magmatism and local domains of anomalous heat flow (e.g., MCMZ) in the axial region of the Belt–Purcell basin, locally accompanied by S-type magmatism and penetrative metamorphic fabrics (McMechan and Price, 1982; Lydon, 2000; McFarlane and Pattison, 2000). Two subsequent weaker, more cryptic Proterozoic orogenic events have been proposed: one at ca 1.0–1.1 Ga (Anderson and Davis, 1995), and another at ca. 900 Ma, the latter associated with regional uplift and block faulting of the Belt–Purcell strata prior to Windermere sedimentation (McMechan and Price, 1982).

3. Geology of the St. Eugene vein system

The St. Eugene vein system occupies two subparallel faults that trend approximately ESE and dip 65° SSW. They cut up-section through the Middle and Upper Aldridge Formations and the lower part of the Creston Formation (Fig. 1b). The vein system has a longitudinal extent of at least 3300 m and a vertical extent of at least 1300 m (Hoy, 1993). The quartz-rich veins range up to 10 m in thickness and contain galena, sphalerite and a range of other sulfide and sulfosalt minerals. The vein system was emplaced in the Mesoproterozoic (Hoy, 1993; Hoy et al., 2000).

The part of the vein and alteration system examined in this study is situated on the east side of Moyie lake, cropping out ~150 m above lake level (the '1100 level' of the mine workings). The outcrop expression of the vein system in this vicinity is shown in Fig. 2a. It is marked by a meter-wide, ESE-trending domain of rusty, discolored rocks that extends variably up the hill slope and transects the gently dipping bedding of the host turbidites. Fig. 2b shows the gently dipping turbidites of the Middle Aldridge Formation several tens of meters away from the vein system. The turbidites show alternating thicker, light colored, sandy beds and thinner, dark colored, argillaceous beds, the latter which develop the mineral assemblages of interest to this study.

3.1. Metamorphosed alteration zones

A ~20 m-wide metasomatic halo is developed in the metaturbidites on either side of the vein system (Joncas and Beaudoin, 2002; see Fig. 1c). Joncas and Beaudoin identified four alteration zones separated by gradational boundaries. The innermost zone is the garnet zone, comprising a variety of garnet-bearing rocks that range from massive garnet + ferroanthophyllite + chlorite + sulfide-bearing assemblages intimately associated with the transecting vein system, to garnet-bearing argillaceous tops of undisturbed turbidite beds such as illustrated in Fig. 2c (Joncas and Beaudoin, 2002; Seitz, 2009). The internal zone contains muscovite-rich mineral assemblages and quartz–chlorite veins, whereas the intermediate zone contains quartz–chlorite ± biotite-bearing veins in a host assemblage similar to the internal zone but not as muscovite-rich (Joncas and Beaudoin, 2002). The external zone is the same as the unaltered regional rocks with the exception of locally disseminated calcite. Joncas and Beaudoin (2002) described isotopic and whole rock compositional trends associated with alteration.

Inclusions of sphalerite, galena and pyrite in the garnet (Joncas and Beaudoin, 2002) indicate that metamorphism post-dated mineralization and hydrothermal alteration, such that the alteration zones are more accurately described as metamorphosed alteration zones. The different hydrothermally-altered bulk compositions responded differently to the metamorphism, resulting in the contrasting mineral assemblages described below.

4. Petrography and chemical analysis

The focus of this study is the argillaceous tops of turbidites, which develop a progression of mineral assemblages related to proximity to the vein system. Out of 15 samples examined under the optical microscope (Seitz, 2009), three were selected for whole rock analysis, mineral chemical analysis, and phase equilibrium modeling: (1) a sample of relatively unaltered argillite collected ~60 m from the vein system (JS-11; see Fig. 1c); (2) a sample of garnetiferous argillite collected within 10 m of the vein system (JS-10; see Figs. 1c and 2c); and (3) a loose sample of sparsely garnetiferous argillite that was not collected from outcrop but whose whole rock composition and modal mineralogy suggest it is intermediate between the other two (JS-1).

4.1. Petrography

All three samples have a fine grained matrix containing muscovite, biotite, quartz, ilmenite and sporadically developed, corroded-looking zoisite, the latter occurring in fine-grained, clear, non-pleochroic, granular grains and aggregates ($\leq$200 μm) with anomalous blue and yellow interference colors (Fig. 2f). The possibility that these grains are clinozoisite cannot be ruled out on optical grounds alone; however, as discussed below in the section on thermodynamic modeling, the distinction is immaterial for the purposes of this paper. Plagioclase is conspicuously lacking. The matrix has a weak, bedding-parallel fabric defined by aligned muscovite (Fig. 2d–f). Biotite occurs in small anhedral porphyroblasts that overprint the matrix fabric (Fig. 2e and f) and display no preferred orientation, suggesting growth under static conditions.

Table 1
Whole rock and mineral compositions.

Wt%	Whole rock major elements			Whole rock trace elements				Wt%	Garnet				Biotite			Chlorite		Muscovite		
	JS-11	JS-1	JS-10	ppm	JS-11	JS-1	JS-10		JS-1 core	JS-1 rim	JS-10 core	JS-10 rim	JS-11	JS-1	JS-10	JS-11	JS-1	JS-11	JS-1	JS-10
SiO_2	52.78	57.69	45.96	BaO	1090	818	1072	SiO_2	36.95	36.49	36.50	37.02	33.84	34.12	34.31	22.90	23.11	46.47	46.54	46.38
TiO_2	1.19	1.00	1.60	Ce	102	158	2	TiO_2	0.06	0.04	0.11	0.01	1.46	1.62	1.67	0.08	0.08	0.33	0.29	0.21
Al_2O_3	28.38	24.50	29.86	Co	<d/l	<d/l	<d/l	Al_2O_3	20.73	20.72	20.47	20.68	17.88	18.29	19.91	21.01	21.53	34.53	34.42	34.16
FeO	2.92	3.86	6.31	Cr2O3	183	241	221	FeO	24.01	24.42	23.35	27.25	25.93	28.06	27.89	33.99	37.01	2.01	2.11	2.99
MnO	0.12	0.12	0.39	Cu	14	9	25	MnO	13.74	9.91	14.22	8.08	0.31	0.16	0.20	0.79	0.50	0.02	0.01	0.00
MgO	0.88	0.70	0.70	Ni	18	122	17	MgO	0.44	0.28	0.35	0.36	5.60	4.61	3.60	8.13	6.67	0.88	0.87	0.79
CaO	0.11	0.09	0.23	Sc	18	18	18	CaO	4.21	7.01	4.20	6.48	0.13	0.00	0.09	n/a	n/a	0.02	0.05	0.04
Na_2O	0.40	0.34	0.40	V	121	99	117	BaO	n/a	n/a	n/a	n/a	0.08	0.07	0.07	n/a	n/a	0.13	0.16	0.10
K2O	8.51	7.30	8.82	Zn	260	250	950	Na_2O	n/a	n/a	n/a	n/a	0.06	0.08	0.02	0.03	0.02	0.34	0.33	0.31
P_2O_5	0.07	0.06	0.07	Ga	32	30	36	K2O	n/a	n/a	n/a	n/a	8.17	8.64	8.53	0.02	0.02	10.69	10.58	10.35
LOI	3.90	3.72	4.43	Nb	25	19	29	F	n/a	n/a	n/a	n/a	0.00	0.02	0.00	n/a	n/a	0.05	0.37	0.12
Total[a]	99.52	99.65	99.14	Pb	103	265	285	H_2O (calc'd)	n/a	n/a	n/a	n/a	3.74	3.78	3.84	10.65	10.77	4.44	4.15	4.37
wt% SO_3	<d/l	0.02	0.14	Rb	294	260	301	Total	100.15	98.87	99.19	99.88	97.20	99.45	100.13	97.60	99.71	99.91	99.88	99.82
				Sr	64	38	48													
				Th	31	28	52													
				U	5	5	7													
				Y	46	74	30													
				Zr	338	330	474													
	Moles of elements × 100								Cations for 12 oxygens				Cations for 11 oxygens			Cations for 14 oxygens		Cations for 11 oxygens		
Si	87.84	96.01	76.49					Si	3.01	2.99	3.00	3.01	2.71	2.70	2.68	2.58	2.57	3.10	3.11	3.11
Ti	1.48	1.25	2.00					Ti	0.00	0.00	0.01	0.00	0.09	0.10	0.10	0.01	0.01	0.02	0.02	0.01
Al	55.67	48.06	58.57					Al	1.99	2.00	1.98	1.98	1.69	1.71	1.83	2.79	2.83	2.72	2.71	2.70
Fe	4.07	5.37	8.78					Fe	1.63	1.67	1.61	1.85	1.74	1.86	1.82	3.20	3.45	0.11	0.12	0.17
Mn	0.16	0.16	0.55					Mn	0.95	0.69	0.99	0.56	0.02	0.01	0.01	0.08	0.05	0.00	0.00	0.00
Mg	2.18	1.74	1.74					Mg	0.05	0.03	0.04	0.04	0.67	0.54	0.42	1.36	1.11	0.09	0.09	0.08
Ca	0.20	0.16	0.41					Ca	0.37	0.62	0.37	0.56	0.01	0.00	0.01	n/a	n/a	0.00	0.00	0.00
Na	1.29	1.10	1.29					Ba	n/a	n/a	n/a	n/a	0.00	0.00	0.00	n/a	n/a	0.00	0.00	0.00
K	18.07	15.50	18.73					Na	n/a	n/a	n/a	n/a	0.01	0.01	0.00	0.01	0.00	0.04	0.04	0.04
P	0.14	0.12	0.12					K	n/a	n/a	n/a	n/a	0.84	0.87	0.85	0.00	0.00	0.91	0.90	0.89
Fe#	0.65	0.76	0.83					Sum	8.00	8.01	8.00	8.00	7.78	7.80	7.73	10.02	10.01	7.00	6.99	7.00
Mn#	0.025	0.022	0.048					Fe#	0.968	0.980	0.974	0.977	0.72	0.78	0.81	0.70	0.76			
Ca#	0.030	0.022	0.036					Xsps	0.32	0.23	0.33	0.18								
A-index[b]	0.13	0.12	0.13					Xgrs	0.12	0.20	0.12	0.19								
								Xalm	0.54	0.56	0.53	0.61								
								Xprp	0.018	0.012	0.014	0.015								

Fe# = Fe/(Mg + Fe).
Mn# = Mn/(Fe + Mg + Mn + Ca).
Ca# = Ca/(Fe + Mg + Mn + Ca).
[a] Including trace elements.
[b] A-index = Al index in Thompson AFM diagram (= moles Al_2O_3 - 3x moles K_2O).
Xsps = Mn/(Fe + Mg + Mn + Ca).
Xgrs = Ca/(Fe + Mg + Mn + Ca).
Xalm = Fe/(Fe + Mg + Mn + Ca).
Xprp = Mg/(Fe + Mg + Mn + Ca).

In addition to the above matrix minerals, sample JS-11 (least altered) contains chlorite porphyroblasts that either occur within, or overprint, the matrix fabric (Fig. 2d). Sample JS-10 (most altered) is chlorite-absent and contains ~3 modal % garnet porphyroblasts, ranging in size from <1 mm to 4 mm (Fig. 2c, e and f). Garnet contains inclusions of ilmenite, quartz and corroded zoisite (Fig. 2f). The inclusions define a linear internal fabric (in two dimensions) in the garnet that is continuous with the linear external matrix fabric, indicating that garnet growth post-dated fabric development (Fig. 2f). The lack of any matrix deformation around the garnet indicates growth under static conditions. Sample JS-1 (intermediate alteration) contains chlorite and sparse (≪1 modal %) garnet.

4.2. Whole rock compositions

Table 1 lists major and trace element compositions of the three rocks, analyzed using methods described in Pattison and Vogl (2005). Going from the unaltered host rocks to the most altered (garnetiferous) rocks, the rocks show increases in: Fe# (= Fe/(Fe + Mg)), from 0.65 to 0.83; Mn# (= Mn/(Mn + Fe + Mg + Ca)), from 0.025 to 0.048; Zn, from 260 to 950 ppm; and Pb, from 103 to 385 ppm. In contrast, chemical parameters that do not show progressive change include Ca, K, Na, Al and the A index of the Thompson (1957) AFM projection (moles Al_2O_3 – 3x moles K_2O); the latter parameter spans the narrow range of 0.02 and −0.02. The lack of variation of these parameters shows that the metasomatism of the argillaceous layers in the turbidites primarily involved addition of Fe and Mn without significant loss or gain of alkalies. This situation is thus ideal to isolate the effects of variations in Fe# and Mn# on garnet stability.

4.3. Mineral compositions

Table 1 lists representative chemical compositions of garnet, chlorite, biotite and muscovite from the three samples. Samples were analyzed on a JEOL 8200 electron microprobe at University of Calgary, using the methods described in Pattison and Vogl (2005). Figs. 3–5 show compositional maps, respectively, of one garnet from sample JS-1 and two garnets from sample JS-10. The garnet in Fig. 4, from sample JS-10, is by far the largest garnet observed in the three

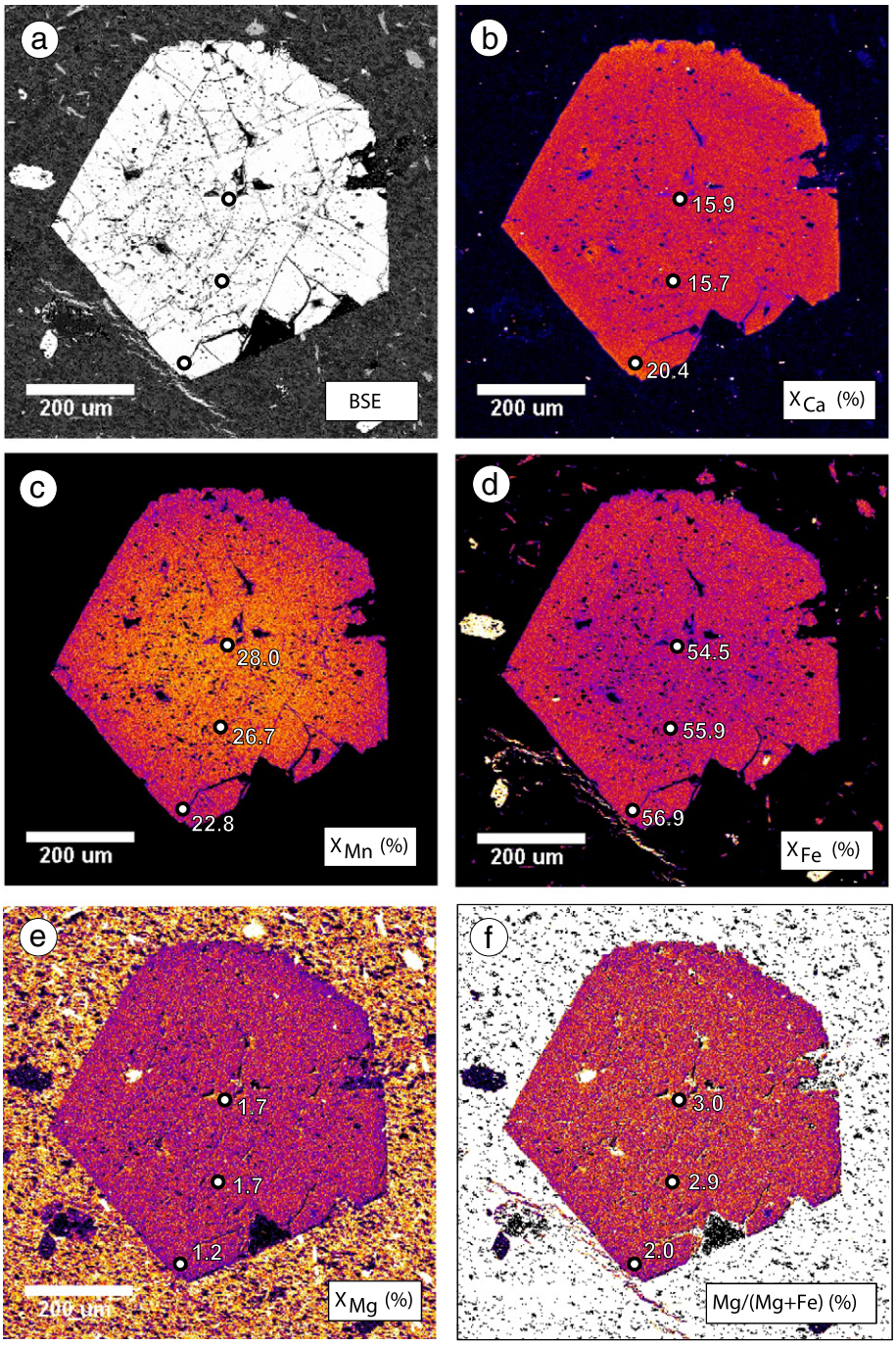

Fig. 3. Sample JS-1. Back scattered electron image and elemental zonation in the largest garnet observed in sample JS-1. (a) Back-scattered electron image with location of quantitative analysis spots. (b) Ca zonation. X_{Ca} (%) = 100 × Ca/(Ca + Fe + Mg + Mn). (c) Mn zonation. X_{Mn} (%) = 100 × Mn/(Ca + Fe + Mg + Mn). (d) Fe zonation. X_{Fe} (%) = 100 × Fe/(Ca + Fe + Mg + Mn). (e) Mg zonation. X_{Mg} (%) = 100 × Mg/(Ca + Fe + Mg + Mn). (f) Zonation in percent Mg/(Mg + Fe).

samples. Photomicrographs of the compositionally mapped garnets in Figs. 4 and 5 are shown in Fig. 2e and f.

Garnet compositions within and between samples JS-1 and JS-10 overlap, with the most extreme zoning preserved in the large garnet in sample JS-10 (Fig. 4). This garnet shows significant core-rim decrease in spessartine content (0.33 to 0.18) and increase in grossular content (0.12 to 0.19), with concomitant increase in almandine content (0.53 to 0.61) and minor change in pyrope content (average pyrope content ~0.015). Grossular content shows an abrupt increase at the outermost rim, a pattern seen in the three mapped garnets from both samples and which is discussed further below. There is no evidence in the zoning of post-peak resorption or diffusional re-equilibration at the garnet rims, consistent with the relatively low metamorphic grade (regional biotite zone). Variations in the Fe# of biotite and chlorite mimic the variations in whole rock composition. Zoisite (possibly clinozoisite) contains negligible Fe.

5. Phase equilibrium modeling

Fig. 6 shows calculated isochemical phase diagram sections for the three rocks. The phase diagrams are modeled in the chemical system MnNCKFMASHT ($MnO–Na_2O–CaO–K_2O–FeO–MgO–Al_2O_3–SiO_2–$

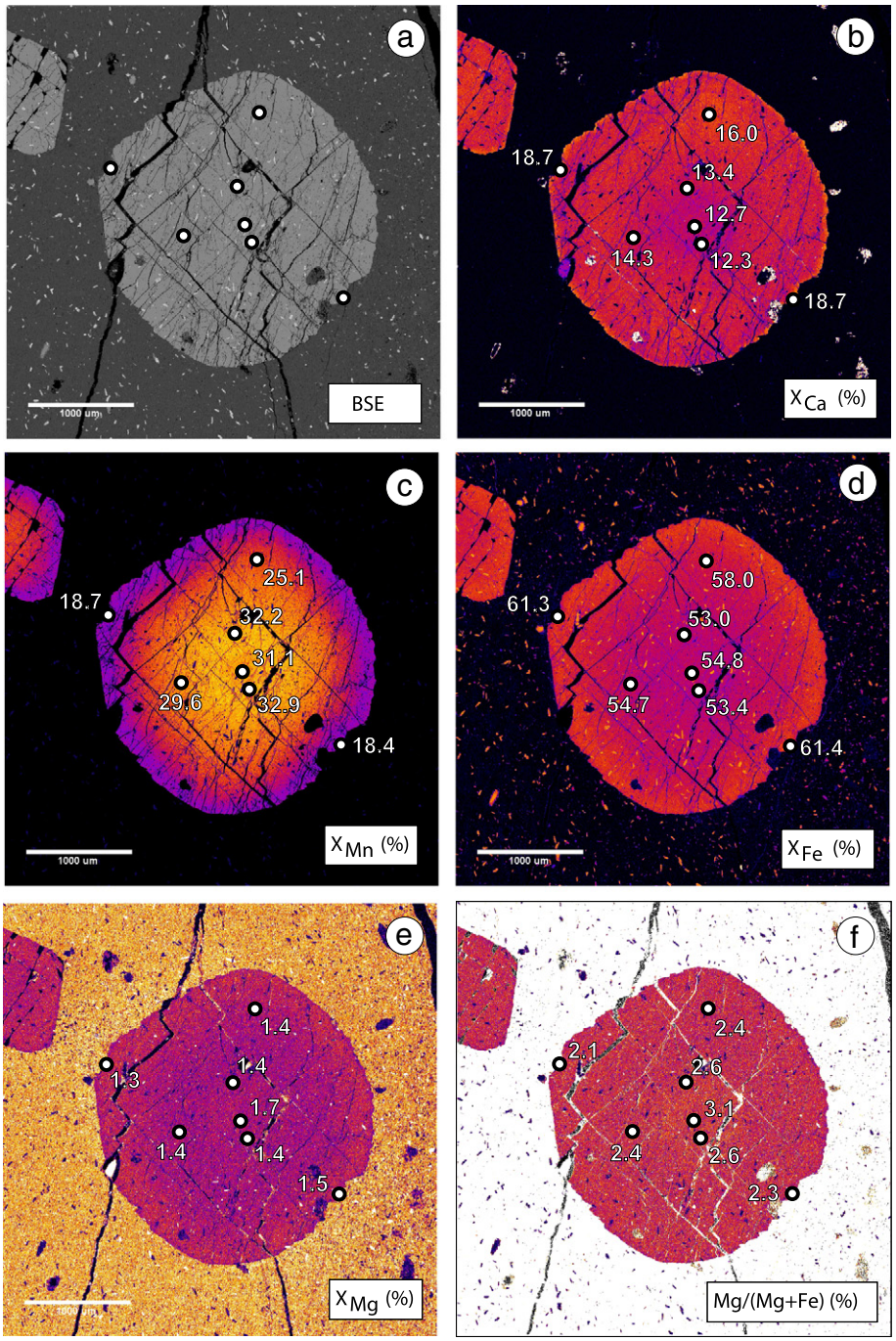

Fig. 4. Sample JS-10. Back scattered electron image and elemental zonation in the largest garnet observed in sample JS-10. Scale bar is 1000 micrometres. Fig. 2e shows a photomicrograph of the garnet. (a) Back-scattered electron image with location of quantitative analysis spots. (b) Ca zonation. X_{Ca} (%) = 100 × Ca/(Ca + Fe + Mg + Mn). (c) Mn zonation. X_{Mn} (%) = 100 × Mn/(Ca + Fe + Mg + Mn). (d) Fe zonation. X_{Fe} (%) = 100 × Fe/(Ca + Fe + Mg + Mn). (e) Mg zonation. X_{Mg} (%) = 100 × Mg/(Ca + Fe + Mg + Mn). (f) Zonation in percent Mg/(Mg + Fe).

H_2O–TiO_2, with C and P_2O_5 deleted from the whole-rock analysis, followed by projection from pyrrhotite; see Pattison and Tinkham, 2009, p. 264–265 for a discussion of choice of chemical system). The phase diagrams were calculated using the Theriak-Domino phase equilibrium modeling software (de Capitani and Brown, 1987; de Capitani and Petrakakis, 2010). The molar bulk compositions of the three rocks used as input to Theriak-Domino are given in Table 1. In the Theriak algorithm, sufficient oxygen is added to the bulk composition to achieve electroneutrality. Fifty moles of hydrogen (equivalent to 25 mol H_2O) were added to the anhydrous bulk composition to ensure that a_{H2O} was unity across the phase diagram (equivalent to aqueous fluid being available as a possible reactant or product across the diagram).

The thermodynamic database used for the calculations is that of Holland and Powell (1998), updated to dataset 5.5 in 2003 that incorporates the Al_2SiO_5 triple point of Pattison (1992). Activity models used in all calculations are those used in Tinkham and Ghent (2005) with the following exceptions: 1) margarite was not considered as a component in white mica, and 2) the ternary feldspar model of Holland and Powell (1998), using a molecular mixing model and asymmetric formalism, was used instead of separate plagioclase and pure orthoclase or sanidine.

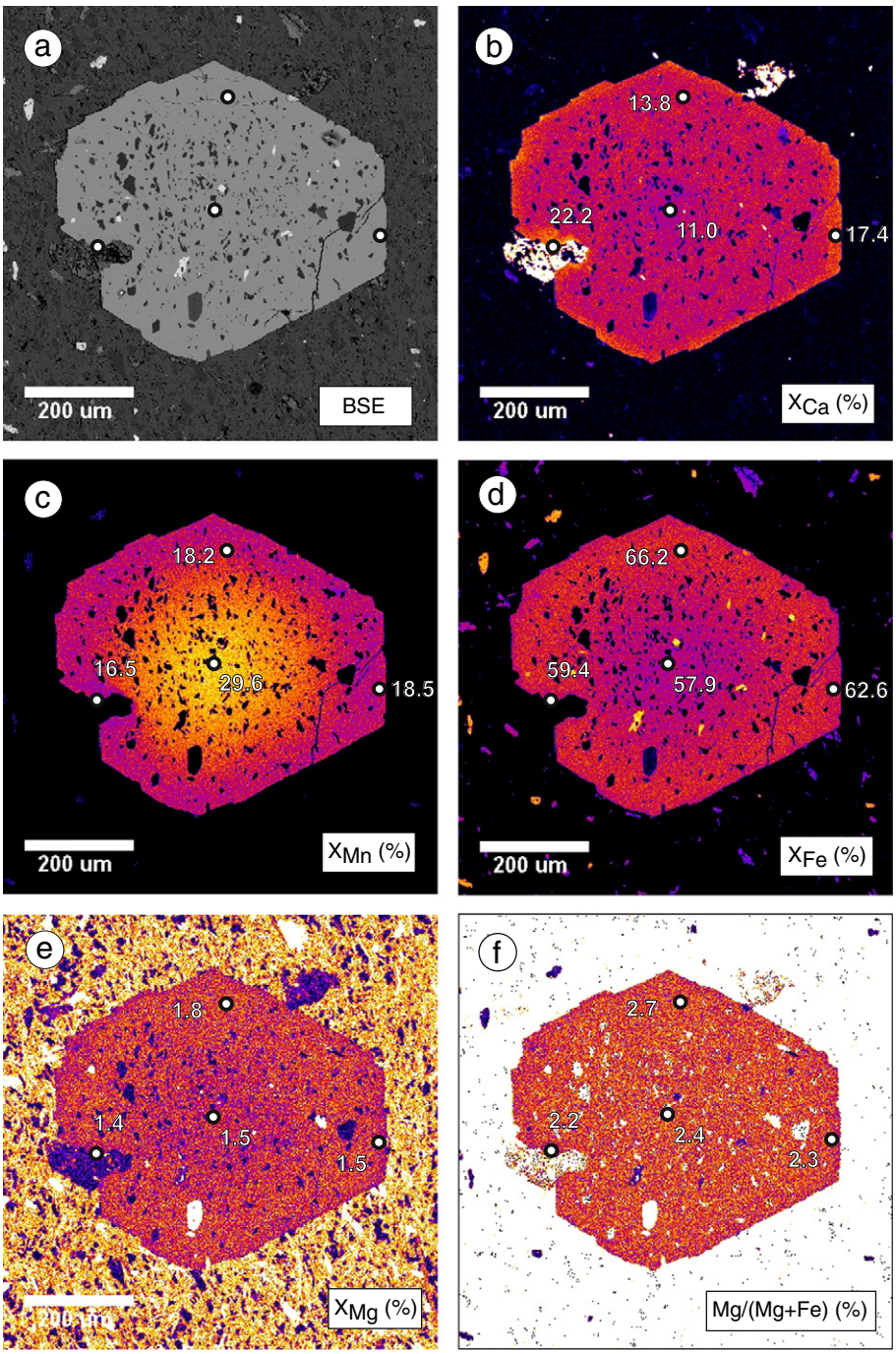

Fig. 5. Sample JS-10. Back scattered electron image and elemental zonation from a small garnet in sample JS-10. Fig. 2f shows a photomicrograph of the garnet. (a) Back-scattered electron image with location of quantitative analysis spots. (b) Ca zonation. X_{Ca} (%) = 100 × Ca/(Ca + Fe + Mg + Mn). (c) Mn zonation. X_{Mn} (%) = 100 × Mn/(Ca + Fe + Mg + Mn). (d) Fe zonation. X_{Fe} (%) = 100 × Fe/(Ca + Fe + Mg + Mn). (e) Mg zonation. X_{Mg} (%) = 100 × Mg/ (Ca + Fe + Mg + Mn). (f) Zonation in percent Mg/(Mg + Fe).

Fig. 6a–c shows isochemical pressure–temperature phase diagram sections for the three samples in order of increasing degrees of alteration (i.e., JS-11, JS-1 and JS-10). Phase boundaries involving zoisite in Fig. 6 are displaced down-temperature by a maximum of 15 °C, usually less than 10 °C, if zoisite is replaced by clinozoisite. The small amount of plagioclase (<0.3 vol.%) predicted to develop at the zoisite-out reaction is calculated to be anorthite rather than the expected anorthite–albite solid solution. This may be an artifact arising from uncertainties in predicted Na–K partitioning in mica, combined with the large amount of muscovite (~80 vol.%) relative to plagioclase in the rocks, giving rise to a modal Ms:Pl ratio of ~250:1.

5.1. Effect of Fe# and Mn# on garnet stability

The most striking feature of the phase diagrams is the progressive increase in predicted stability of garnet with increasing degree of alteration. In JS-10, the most altered rock, the lower limit of garnet stability is ~100 °C and 2–3 kbar lower than in JS-11, the least altered rock.

An attempt was made to separate the effects of variation in Fe# and variation in Mn# on garnet stability (see Fig. 6d). Mahar et al. (1997) and Caddick and Thompson (2008) performed a similar exercise using a forward-modeling approach for average rock compositions. The approach adopted in this study is as follows. The

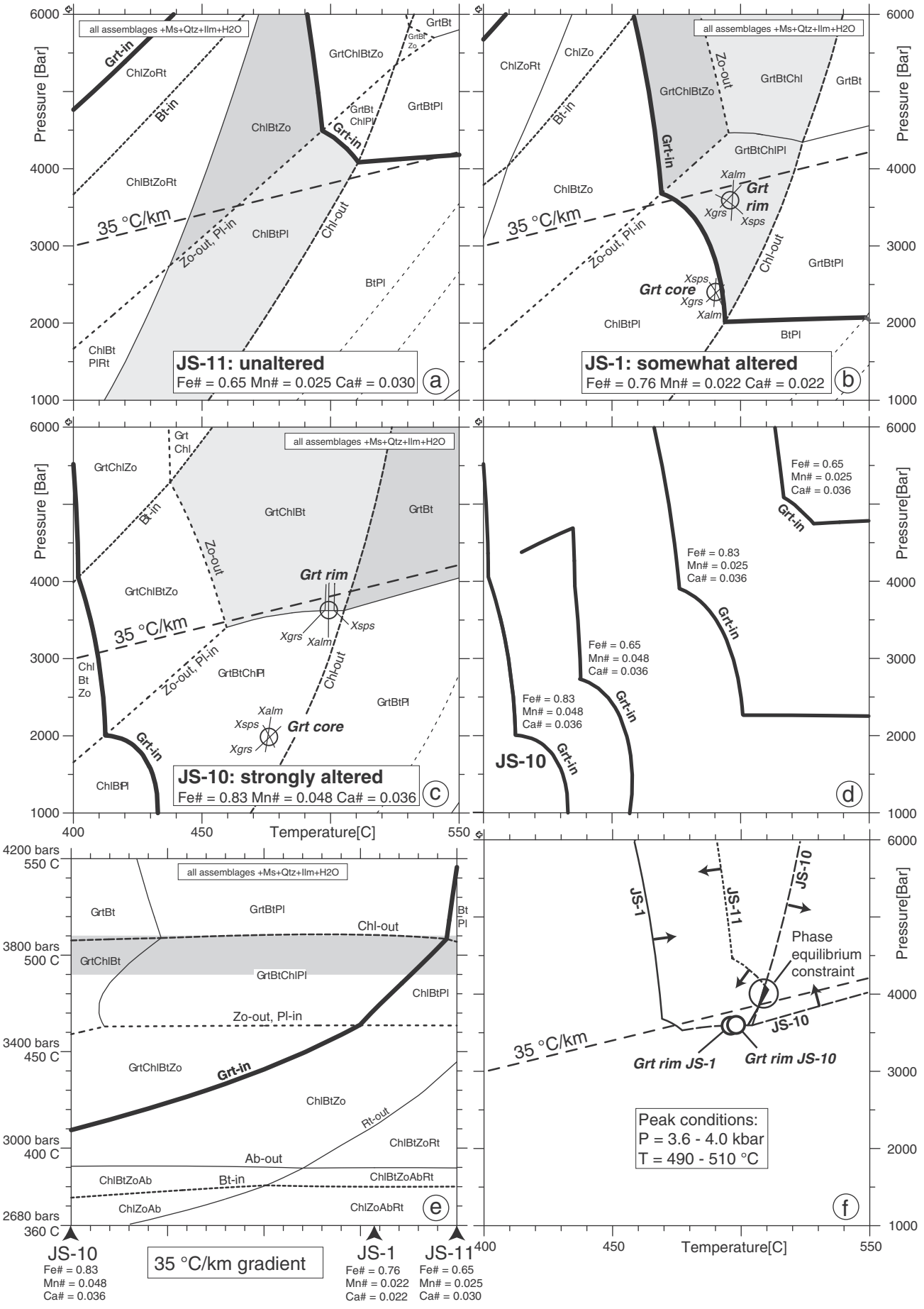
all assemblages +Ms+Qtz+Ilm+H2O
Grt-in
Bt-in
Zo-out, Pl-in
Chl-out
Zo-out
Rt-out
Ab-out
35 °C/km
ChlZoRt
GrtChlBtZo
GrtBt
GrtBtPl
ChlBtZo
ChlBtZoRt
ChlBtPl
BtPl
ChlBt PlRt
GrtBtChl
GrtBtChlPl
Grt rim
Grt core
Xalm
Xgrs
Xsps
JS-11: unaltered
Fe# = 0.65 Mn# = 0.025 Ca# = 0.030
JS-1: somewhat altered
Fe# = 0.76 Mn# = 0.022 Ca# = 0.022
JS-10: strongly altered
Fe# = 0.83 Mn# = 0.048 Ca# = 0.036
Fe# = 0.65 Mn# = 0.025 Ca# = 0.036
Fe# = 0.83 Mn# = 0.025 Ca# = 0.036
Fe# = 0.65 Mn# = 0.048 Ca# = 0.036
Fe# = 0.83 Mn# = 0.048 Ca# = 0.036
JS-10
Pressure [Bar]
Pressure[Bar]
Temperature[C]
4200 bars 550 C
3800 bars 500 C
3400 bars 450 C
3000 bars 400 C
2680 bars 360 C
GrtChlBt
ChlBtPl
ChlBtZoAb
ChlBtZoAbRt
ChlZoAb
ChlZoAbRt
JS-1
JS-11
Phase equilibrium constraint
Grt rim JS-1
Grt rim JS-10
Peak conditions:
P = 3.6 - 4.0 kbar
T = 490 - 510 °C
35 °C/km gradient
JS-10
Fe# = 0.83
Mn# = 0.048
Ca# = 0.036
JS-1
Fe# = 0.76
Mn# = 0.022
Ca# = 0.022
JS-11
Fe# = 0.65
Mn# = 0.025
Ca# = 0.030
a
b
c
d
e
f

whole rock composition of the most altered rock, JS-10, was modified: first, by changing the Mn content to be the same as in JS-11, with all other parameters in JS-10 including Mg and Fe content unchanged; second, by changing the Mg and Fe content to be the same as in JS-11, with all other parameters in JS-10 including Mn content unchanged; and third, by changing Mn, Mg and Fe content to be the same as in JS-11, with all other parameters in JS-10 unchanged. The position of the garnet-in line for JS-10 and for the above three scenarios is shown in Fig. 6d. The garnet-in line for the third scenario is close to, although not identical, to the garnet-in line for sample JS-11, showing that variation in Fe# and Mn# accounts for most of the difference in garnet stability between the most altered and least altered rocks.

With respect to the unmodified composition of JS-10, varying the Mn# first (scenario 1) results in 60% of the total displacement to the position represented by scenario 3, with the remaining 40% accounted for by the change in Fe#. Varying the Fe# first results in 25% of the total displacement to the position represented by scenario 3, with the remaining 75% accounted for by the change in Mn#. Averaging the two, about 2/3 of the increase in garnet stability is accounted for by the difference in Mn# and 1/3 by difference in Fe#.

Fig. 6e shows a binary T(P)–X diagram for a P–T path along the dashed geothermal gradient in Fig. 6a–f, in which the two compositional end members are the most altered and least altered rocks, respectively, i.e. samples JS-10 and JS-11. The smooth down-T(P) expansion of garnet stability with increasing degree of alteration is clearly shown. The general result is the same for other reasonable P–T paths. The intermediate sample, JS-1, although not falling exactly on the binary, can be placed on the diagram to satisfy the observed mineral assemblage constraints. Fig. 6e is useful in visualizing the predicted parallel, but independent, prograde evolution of mineral assemblages in the metasomatically altered argillites surrounding the St. Eugene vein system.

6. Pressure–temperature estimation and kinetic effects on mineral development

The following section addresses the estimation of pressure–temperature conditions at St. Eugene through comparison of the mineral assemblages, compositions and zoning of the natural samples with the calculated phase diagrams in Fig. 6. A number of aspects of the natural samples suggest that kinetic factors influenced the development of the mineral assemblages, complicating interpretation of the pressure–temperature conditions.

6.1. Pressure–temperature estimation using mineral assemblages: the effect of metastable zoisite breakdown

An estimate of the peak P–T conditions at St. Eugene can in principle be obtained by plotting the observed mineral assemblages of the three rocks on the phase diagrams in Fig. 6a–c, and looking for the P–T area of overlap (Fig. 6f). The dark gray domains in Fig. 6a–c show where the observed mineral assemblages plot in the respective phase diagrams.

A complication in this approach is the possibility of metastable persistence of some phases, as suggested by the absence of a stability field for the observed mineral assemblage Grt + Zo + Bt in sample JS-10. In Fig. 6c, the terminal stability of zoisite is predicted to occur ~50 °C down-temperature of the terminal stability of chlorite, yet zoisite occurs in the chlorite-free rock (see Figs. 2f, 4 and 5). At the relatively low metamorphic temperatures of the regional biotite zone, sluggish dissolution of zoisite may have resulted in its metastable persistence upgrade of where it is predicted to be consumed according to equilibrium processes. The corroded nature of the zoisite in the rocks (Fig. 2f), and the relatively abrupt increase in Ca content at the outmost rims of garnet (Figs. 4 and 5), may be evidence for overstepped reaction of zoisite at the latter stage of garnet growth. Support for this view comes from comparison of the garnet zoning with calculated equilibrium isopleths of grossular content of garnet (Fig. 7a): the observed trend of increasing Ca-content in garnet from core to rim is the opposite to that predicted by up-temperature passage across isopleths of decreasing Ca-content in Fig. 7a.

Fig. 7b shows a phase diagram for sample JS-10 calculated in the Ca-free MnNKFMASHT chemical system, simulating a situation in which zoisite is wholly unreactive during initial garnet growth. The diagram was calculated by setting Ca to zero in the bulk composition of sample JS-10 listed in Table 1. Compared to the Ca-bearing phase diagrams in Figs. 6c and 7a, the garnet-in line is displaced up-temperature by ~50 °C. Reality must lie between these end-members because some Ca is contained in the garnet cores, suggesting either slow release of Ca from slowly dissolving zoisite during initial garnet growth, or participation of some other Ca-mineral no longer present in the rock. More substantial zoisite consumption appears to have been delayed until later in garnet growth, as suggested by the Ca-rich rims.

Stoichiometries of the zoisite-bearing and zoisite-free garnet-producing reactions were calculated by subtracting the calculated modes for two different P–T points along the metamorphic gradient within the Grt + Zo + Chl + Bt field in Fig. 6c and the Grt + Chl + Bt field in Fig. 7b, respectively. The results were normalized to 1 mol of garnet. The zoisite-bearing reaction is:

$$1.15\mathrm{Ms} + 1.00\mathrm{Chl} + 0.06\mathrm{Ilm} + 0.50\mathrm{Zo} = 1\mathrm{Grt} + 1.70\mathrm{Bt} + 1.23\mathrm{Qtz} + 3.72\mathrm{H_2O}. \quad (1)$$

The zoisite-absent reaction is:

$$1.92\mathrm{Ms} + 1.77\mathrm{Chl} + 0.09\mathrm{Ilm} = 1\mathrm{Grt} + 2.93\mathrm{Bt} + 0.96\mathrm{Qtz} + 6.06\mathrm{H_2O} \quad (2)$$

The main difference between the reactions is the greater involvement of micas and chlorite in the zoisite-free reaction, resulting in a greater amount of water released.

Prograde unreactivity and metastable persistence of porphyroblasts such as garnet, staurolite and chloritoid have been documented in other areas (e.g., Waters and Lovegrove, 2002; Pattison and Tinkham, 2009; Pattison et al., 2011 and references therein). Most of these examples are of higher metamorphic grade than at St. Eugene (middle amphibolite facies vs. transitional greenschist-amphibolite facies). The lower temperatures at St. Eugene increase the expected degree of porphyroblast unreactivity, owing to the exponential

Fig. 6. (a)–(c) Isochemical phase diagram sections for sample JS-11 (least altered), JS-1 (somewhat altered) and JS-10 (most altered). See text for calculation details. Whole rock and garnet compositions are listed in Table 1. Shaded domains are where the observed mineral assemblages plot (see text for details). For the whole rock compositions, Fe# = Fe/(Fe + Mg); Mn# = Mn/(Mn + Fe + Mg + Ca); Ca# = Ca/(Ca + Fe + Mg + Mn). For the garnet isopleth intersections, Xsps = Mn/(Mn + Fe + Mg + Ca), Xgrs = Ca/(Mn + Fe + Mg + Ca) and Xalm = Fe/(Mn + Fe + Mg + Ca). Abbreviations from Kretz (1983). Dashed 35 °C/km geothermal gradient assumes rock density of 2.7 g/cm^3. (d) Displacement of the garnet-in line for sample JS-10 for different values of Mn# and Fe# (see text for details). (e) Binary T(P)–X diagram along a linear 35 °C/km P–T path, with the two compositional end members represented by samples JS-10 and JS-11 (most altered and least altered, respectively). The horizontal gray band is the estimated temperature range of peak metamorphism (490–510 °C). The composition of sample JS-1 does not lie exactly on the binary between JS-10 and JS-11, but is placed in Fig. 6e to satisfy the predicted mineral assemblage sequence along the 35 °C/km P–T path illustrated in Fig. 6b. (f) Synthesis of mineral assemblage constraints from samples JS-1, JS-10 and JS-11, and location of garnet rim isopleth intersections.

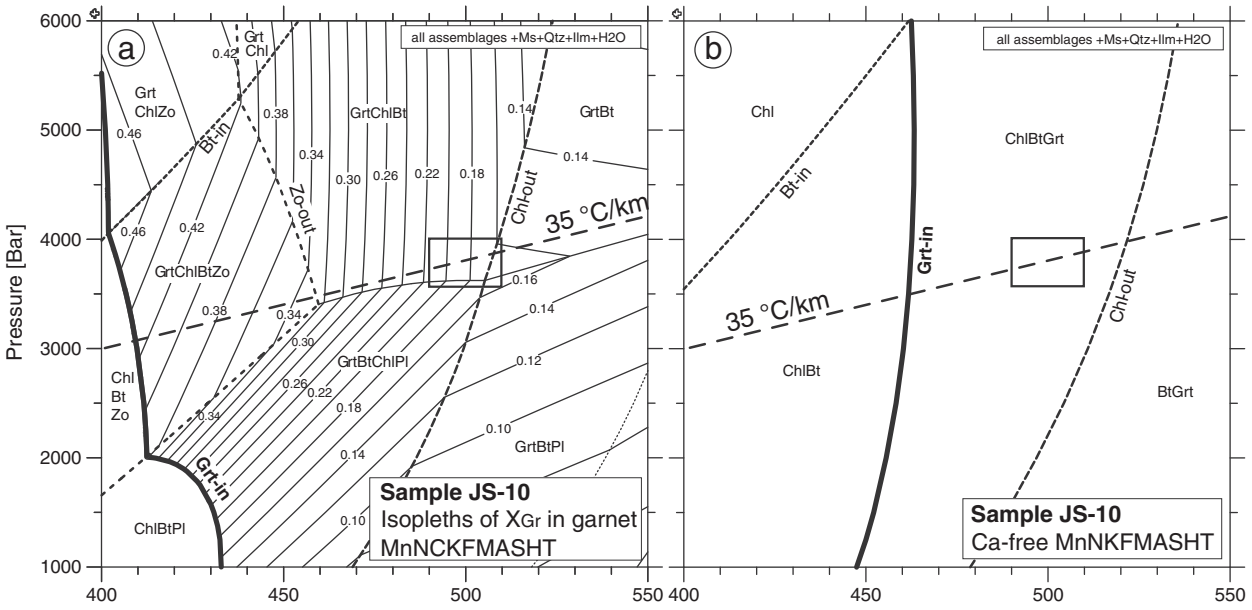

Fig. 7. (a) Calculated equilibrium isopleths of grossular content of garnet for sample JS-10 (compare to Fig. 6c). Grossular content = Ca/(Ca + Fe + Mg + Mn). Box represents estimated range of peak P–T conditions from Fig. 6f. (b) Isochemical phase diagram section for sample JS-10, calculated for the Ca-free MnNKFMASHT chemical system. See text for calculation details. Box represents estimated range of peak P–T conditions from Fig. 6f.

decrease in rates of interface processes and transport processes with decreasing temperature according to the Arrhenius relation.

In summary, for analysis of P–T conditions at St. Eugene using mineral assemblages, more weight is placed on the absence of chlorite in JS-10 than on the presence of zoisite. Using similar reasoning, whereas the observed mineral assemblage of samples JS-1 and JS-11 plot in the dark gray domains in Fig. 6a and b, the possibility of metastable persistence of zoisite means that the rocks may have attained P–T conditions above the terminal stability of zoisite (light gray domains in Fig. 6a and b).

Fig. 6f shows that there is a small area of P–T overlap between the three mineral assemblages (light gray domains) at ~4.0 kbar, 510 °C. The apparent tightness of the constraint likely exaggerates the real precision of the estimate. Waters and Lovegrove (2002) and Powell and Holland (2008) discussed the numerous sources of error in the calculation of phase diagram sections and the assessment of natural mineral assemblages therein. For St. Eugene, a realistic estimate of uncertainty is at least ±0.5 kbar and ±25 °C, but unlikely to be more than ±1.0 kbar and ±50 °C.

As a test of the 4.0 kbar, 510 °C P–T estimate, garnet modes were calculated for garnet-bearing samples JS-1 and JS-10 using Theriak. These were compared to the observed modes, recognizing that the possible kinetic factors noted above lead to some uncertainties in the analysis of the natural samples. The predicted and measured modes turn out to be in very close agreement (3 modal percent garnet in JS-10 and ≪1 modal percent garnet in JS-1), adding confidence to the P–T estimate. Calculated modes for other P–T conditions within the ±0.5 kbar, ±25 °C uncertainty range are not significantly different.

6.2. Pressure–temperature estimation using garnet rim compositions: equilibrium vs. fractional processes and the effect of metastable zoisite breakdown

Pressure–temperature estimates can in principle be obtained from intersection of compositional isopleths on phase diagrams (e.g., Powell and Holland, 2008). Isopleths of garnet end members (spessartine, grossular, almandine) were calculated for the two garnet-bearing samples, JS-1 and JS-10, using Theriak-Domino. Core and rim compositions from the analyzed garnets (Table 1) were plotted on the isopleth diagrams and the resulting isopleth intersections plotted in Fig. 6b and c. In the absence of post-peak diffusional re-equilibration, rim compositions are expected to give the best estimate of peak P–T conditions. Garnet rims from both JS-10 and JS-11 yield tight isopleth intersections that are close to coincident at ~3.6 kbar, 495 °C, close to the P–T area of overlap of the mineral assemblages (Fig. 6f).

A caveat in using this approach is the process of fractionation associated with garnet growth, which changes the effective bulk composition and therefore the position of phase boundaries and isopleths. Garnet fractionation along the dashed geothermal gradient in Fig. 6, assuming perfect equilibrium in the matrix assemblage, was therefore performed using Theriak-Domino. The results vary modestly for other reasonable P–T paths. In the case of weakly garnetiferous sample JS-1, in which the garnet-in line is <30 °C and <0.5 kbar from the ~4 kbar, 500 °C phase equilibrium estimate (Fig. 6b), and the modal amount garnet produced is <1%, the effect of garnet fractionation on isopleth positions is negligible. For garnet-richer sample JS-10, fractionation resulted in loss of Ca from the matrix assemblage well (~40 °C) below the estimated peak conditions, prohibiting an assessment of isopleth displacement. Predicted loss of matrix Ca in sample JS-10 is at odds with the presence of zoisite in the rock and the observed enrichment of Ca at garnet rims.

The possibility of metastable breakdown of zoisite further complicates interpretation of the calculated Ca isopleths. For sample JS-10, the equilibrium Ca isopleths in the vicinity of 4 kbar, 500 °C are located in a zoisite-free stability field well up-grade of the predicted zoisite-out reaction (Fig. 7a). If the Ca-enrichment at the garnet rims is due to metastable zoisite breakdown at these conditions, the equilibrium Ca isopleths will underestimate the Ca-content of the garnet formed by the metastable reaction. An attempt was made to estimate the predicted Ca-content of garnet produced in a metastable zoisite-consuming reaction by extrapolating the trend of Ca isopleths in the Grt + Zo + Bt + Chl field of Fig. 7a up-temperature to 500 °C. The predicted grossular values are ~0.27, much higher than the observed range of 0.18–0.22 (Figs. 3–5). As argued above, reality may lie between these two end members.

In summary, the P–T estimates from garnet rim isopleth intersections and phase equilibrium constraints are in close agreement, spanning a range of 3.6–4.0 kbar and 490–510 °C. However, the

incompletely understood extent of fractionation and of other disequilibrium processes (in particular metastable zoisite breakdown) on the P–T estimates renders them uncertain in a way that is not easy to quantify.

6.3. Interpretation of garnet core compositions and the effect of reaction overstepping

Garnet core compositions from samples JS-1 and JS-10 yield tight isopleth intersections of 2.0 kbar, 475 °C and 2.4 kbar, 490 °C, respectively (Fig. 6b and c). Assuming equilibrium, isopleth intersections from garnet cores should give an estimate of the P–T conditions of garnet growth (Tinkham and Ghent, 2005). The results according to this assumption are problematic. An extreme geothermal gradient of ~60 °C/km is implied, more akin to the contact zones of magmatic intrusions than in the broad, regional domain of relatively low grade regional metamorphism surrounding St. Eugene. Combining these P–T estimates with the approximate peak P–T conditions of 3.6–4.0 kbar, 490–510 °C yields a peculiar prograde P–T path involving near-isothermal 1.52.0 kbar pressure increase (equivalent to 5–7 km of burial accompanied by less than 20 °C of temperature increase). Such a P–T path would imply garnet growth during rapid tectonic burial (e.g., thrust-thickening) of the Belt–Purcell sediments in the Mesoproterozoic, for which there is no geological or structural evidence (McMechan and Price, 1982). In addition, thermal modeling (e.g., England and Thompson, 1984) predicts that tectonic burial of this magnitude would be followed by temperature increase in response to thermal re-equilibration, at odds with the preserved low grade mineralogy, textures and zoning of the St. Eugene rocks.

An alternative interpretation of the garnet core isopleth intersections is that they also reflect disequilibrium processes. Separate from the possible unreactivity of zoisite, initial garnet formation may have been overstepped due to kinetic inhibitions to nucleation and growth. Overstepping of initial garnet formation from a muscovite + chlorite-rich matrix has been documented in several contact and regional settings (see summary in Pattison et al., 2011). In the Nelson aureole, initial garnet formation predicted to occur at ~530 °C was delayed until ~560 °C (Pattison and Tinkham, 2009; Gaidies et al., 2011). At St. Eugene, both the peak temperature (~500 °C) and the predicted temperatures of the garnet-in reaction (~410 °C and ~470 °C for samples JS-10 and JS-1, respectively; Fig. 6) are lower than at Nelson.

The magnitude of overstepping caused by kinetic barriers to nucleation and growth is related to the rate at which the chemical driving force for reaction (reaction affinity) builds as the reaction is overstepped. This energy is used to overcome the kinetic barriers to nucleation and growth (Waters and Lovegrove, 2002; Pattison et al., 2011). For thermal overstepping, the rate of buildup of reaction affinity is equal to the entropy change of reaction. Entropy changes of the chlorite-consuming, garnet-forming reactions at St. Eugene were calculated using the approach described in Pattison et al. (2011). The entropy of reaction for the zoisite-bearing and zoisite-absent reactions (reactions 1 and 2) are 8.0 and 9.8 J/°C of overstep, respectively, normalized to 1 mol of oxygen in garnet. These are similar to the 10.3 J/°C value for the garnet-forming reaction in the Nelson aureole (Table 1 of Pattison et al., 2011). Given the relatively low temperature and lack of deformation at St. Eugene, thermal overstepping of garnet nucleation may therefore be expected. The maximum thermal overstep at St. Eugene is the difference between the peak temperature and the temperature of the equilibrium garnet-in reaction, which for samples JS-10 and JS-1 yields maximum oversteps of ~90 °C and ~30 °C, respectively (Fig. 6b and c). For reaction 2 in the Ca-free system (Fig. 7b), the maximum overstep would be ~40 °C.

Gaidies et al. (2011) showed how increasing degrees of overstepping may lead to to increasing degrees of mismatch between equilibrium garnet compositions and those that form from overstepped reaction. Applying this approach to a garnet zone sample from the Nelson aureole, they showed how measured core compositions of overstepped garnets, when plotted assuming growth under equilibrium conditions, implied implausibly low pressures, reminiscent of the results of this study. A more complete treatment of the possible compositional effects of reaction overstepping and zoisite unreactivity at St. Eugene awaits future study.

6.4. Summary of pressure–temperature estimates and tectonic implications

Based on the similarity of P–T estimates from mineral assemblages and garnet rim isopleth intersections, we interpret the peak P–T conditions at St. Eugene to have been approximately 3.6–4.0 kbar, 490–510 °C. A conservative estimate of the uncertainty in pressure is ±1 kbar, owing to a combination of thermodynamic uncertainties and the fractionation and disequilibrium factors discussed above, the latter two which affect especially the pressure-sensitive garnet Ca isopleths. The St. Eugene estimate is similar to the 3.8 kbar, 450 °C estimate from the Sullivan Mine, where, like St. Eugene, garnet occurs in hydrothermally-altered rocks in a domain of regional biotite zone conditions. The inferred St. Eugene pressure is also similar to the 3.5–4.0 kbar pressure estimate from the Matthew Creek Metamorphic Zone.

The mean P–T estimate at St. Eugene of 3.8 kbar, 500 °C, combined with a mean rock density of 2.7 g/cm^3, implies an average (linear) geothermal gradient of ~ 35 °C/km, consistent with burial metamorphism in a rift-related extensional environment (see 'Metamorphism' section above). On the other hand, accounting for 3.8 kbar (~14 km) of pre-Windermere overburden at the time of metamorphism at St. Eugene is difficult. The 3.5–4.0 kbar metamorphic rocks at Matthew Creek and Sullivan are hosted, respectively, in the Lower Aldridge Formation and at the Lower–Middle Aldridge Formation boundary. These rocks are covered by, respectively, an estimated 12–14 and 10–12 km of Belt–Purcell strata (Hoy, 1993; Hoy et al., 2000; Lydon, 2000). In contrast, the rocks at St. Eugene are hosted in the upper part of the Middle Aldridge Formation, implying less than ~8 km (~2.2 kbar) of Belt–Purcell overburden according to the stratigraphic estimates of Hoy et al. (2000).

Possible explanations are various and include the following, individually or in combination: (1) inaccurate (too high) estimation of pressure, perhaps related to the thermodynamic uncertainties and kinetic effects noted above; (2) underestimation of the stratigraphic thickness of the Belt–Purcell overburden; and (3) unrecognized Mesoproterozoic tectonic thickening of a more subtle variety than the near-isothermal loading implied by the apparent garnet core-rim P–T path.

7. Discussion

7.1. Petrologic significance of St. Eugene garnet-bearing rocks

The St. Eugene rocks provide an excellent natural complement to theoretical treatments of garnet stabilization by Mn and Fe (e.g., Atherton, 1977; Loomis, 1986; Spear, 1988; Spear and Cheney, 1989; Symmes and Ferry, 1992; Droop and Harte, 1995; Mahar et al., 1997; Tinkham et al., 2001; Wei et al., 2004; Caddick & Thompson, 2008). The results from St. Eugene, in which garnet is stabilized by >100 °C in rocks high in Fe/(Fe + Mg) and Mn relative to unaltered metapelite, are compatible with the findings of these earlier studies.

A special, possibly unique, feature of the St. Eugene rocks is the variation in Mn# and Fe# without significant variation in alkalies and aluminum, as revealed by the nearly uniform A-index values of the rocks in the Thompson (1957) AFM projection. Separating the effects of Mn# and Fe# on garnet stability shows that although both chemical parameters are important, Mn has the stronger effect.

7.2. Controls on garnet-bearing rocks in the Purcell Anticlinorium

The results of this study suggest that the locally developed garnet-bearing rocks at St. Eugene reflect unusual bulk compositions rather than a local domain of higher metamorphic grade. The P–T conditions of formation are consistent with the ambient biotite zone mineral assemblages developed in the 'normal', unaltered metaturbidites surrounding the deposit, the latter represented by sample JS-11. The garnet-bearing rocks of St. Eugene are therefore like those of Sullivan, Fors, Mt. Mahon and deposits of the Coeur d'Alene district (see Introduction), rather than like the obviously higher grade garnet-bearing schists of the Matthew Creek Metamorphic Zone.

7.3. Garnet as a vector to mineralization

The restriction of garnet to altered rocks suggests that it is a good indicator, or 'vector', to localities affected by hydrothermal activity (cf. Joncas and Beaudoin, 2002). Although not all garnet-bearing, hydrothermally altered rocks are associated with economic mineralization, most of the economic hydrothermal mineral deposits in the Purcell Anticlinorium do contain garnet.

Garnet is only effective as a vector to hydrothermal alteration and possible mineralization under certain metamorphic conditions. The ideal metamorphic conditions are within ~100 °C and ~2–3 kbar of the lower limit of garnet stability in normal (unaltered) rock compositions, i.e. high enough grade that garnet will develop in altered rock compositions but not unaltered rock compositions, yet low enough grade that garnet is not widespread as a metamorphic mineral in normal (unaltered) rock compositions. These conditions correspond to the metamorphic chlorite and biotite zones (greenschist and lower amphibolite facies), exactly the metamorphic conditions of the Belt–Purcell Supergroup of the southern Purcell Anticlinorium. Other garnet-bearing localities in the Purcell Anticlinorium, and in comparable domains of low grade metamorphism in other orogenic belts, therefore deserve careful investigation from both academic and exploration perspectives.

Acknowledgments

This research was supported by NSERC Discovery Grant 037233 to Pattison. We thank Peter Klewchuk for providing advice during the initial field work at St. Eugene, Mickey Horvath for preparation of thin sections, and Rob Marr for help with the electron microprobe. We thank an anonymous reviewer and especially Mark Caddick for their reviews.

References

Anderson, H.E., Davis, D.W., 1995. U–Pb geochronology of the Moyie Sills, Purcell Supergroup, southeastern British Columbia: implications for the Mesoproterozoic geological history of the Purcell (Belt) Basin. Canadian Journal of Earth Sciences 32, 1180–1193.

Anderson, H.E., Goodfellow, W.D., 2000. Geochemistry and isotope chemistry of the Moyie Sills: implications for the early tectonic setting of the Mesoproterozoic Purcell basin. In: Lydon, J.W., Hoy, T., Slack, J.F., Knapp, M. (Eds.), The geological environment of the Sullivan deposit, British Columbia: Geological Association of Canada, Mineral Deposits Division, Special Publication, 1, pp. 302–321.

Anderson, H.E., Parrish, R.R., 2000. U–Pb geochronological evidence for the geological history of the Belt–Purcell Supergroup, southeastern British Columbia. In: Lydon, J.W., Hoy, T., Slack, J.F., Knapp, M. (Eds.), The geological environment of the Sullivan deposit, British Columbia: Geological Association of Canada, Mineral Deposits Division, Special Publication, 1, pp. 113–126.

Atherton, M.P., 1977. The metamorphism of the Dalradian rocks of Scotland. Scottish Journal of Geology 13, 331–370.

Berry, A.D., 1951. A study of the Aldridge Formation, St. Mary Lake area, British Columbia. Unpublished MSc thesis, University of Alberta.

Britton, J.M., Pighin, D.L., 1995. Fors — a Proterozoic sedimentary exhalative base metal deposit, Purcell Supergroup, southeastern British Columbia (82G/5W). In: Grant, B., Newell, J.M. (Eds.), Geological fieldwork 1994: British Columbia Ministry of Energy, Mines and Petroleum Resources Paper 1995-1, pp. 99–109.

Brown, D.A., 1998. Geological Compilation of the Yahk (East Half) and Yahk River (West Half) Map Areas, Southeastern British Columbia (82F/1E, 82G/4W). British Columbia Ministry of Energy and Mines, Geoscience Map 1998–2,1:50,000 scale.

Brown, D.A., Stinson, P., 1995. Geological mapping of the Yahk map area, southeastern British Columbia: an update. In: Grant, B., Newell, J.M. (Eds.), Geological fieldwork 1994: B.C. Ministry of Energy, Mines and Petroleum Resources Paper 1995-1, pp. 111–125.

Caddick, M.J., Thompson, A.B., 2008. Quantifying the tectono-metamorphic evolution of politic rocks from a wide range of tectonic settings: mineral compositions in equilibrium. Contributions to Mineralogy and Petrology 156, 177–195.

Carlson, W.D., 2002. Scales of disequilibrium and rates of equilibration during metamorphism. American Mineralogist 87, 185–204.

Chernoff, C.B., Carlson, W.D., 1997. Disequilibrium for Ca during growth of pelitic garnet. Journal of Metamorphic Geology 15, 421–438.

de Capitani, C., Brown, T.H., 1987. The computation of chemical equilibria in complex systems containing non-ideal solutions. Geochimica et Cosmochimica Acta 51, 2639–2652.

de Capitani, C., Petrakakis, K., 2010. The computation of equilibrium assemblage diagrams with Theriak/Domino software. American Mineralogist 95, 1006–1016.

De Paoli, G.R., Pattison, D.R.M., 1995. Metamorphic pressure, temperature and fluid composition of rocks of the Sullivan Mine, Kimberley, B.C., using silicate–carbonate equilibria. Canadian Journal of Earth Sciences 32, 1937–1949.

De Paoli, G.R., Pattison, D.R.M., 2000. Thermobarometric calculation of peak metamorphic conditions of the Sullivan deposit. In: Lydon, J.W., Hoy, T., Slack, J.F., Knapp, M. (Eds.), The geological environment of the Sullivan deposit, British Columbia: Geological Association of Canada, Mineral Deposits Division, Special Publication, 1, pp. 272–280.

Droop, G.T.R., Harte, B., 1995. The effect of Mn on the phase relations of medium-grade pelites: constraints from natural assemblages on petrogenetic grid topology. Journal of Petrology 36, 1549–1578.

Doughty, P.T., Chamberlain, K.R., 1996. Salmon River Arch revisited; new evidence for 1370 Ma rifting near the end of deposition in the middle Proterozoic Belt Basin. Canadian Journal of Earth Sciences 33, 1037–1052.

England, P.C., Thompson, A.B., 1984. Pressure-temperature-time paths of regional metamorphism. I. Heat transfer during the evolution of regions of thickened continental crust. Journal of Petrology 25, 894–928.

Frycklund Jr., V.C., 1964. Ore deposits of the Coeur d'Alene district, Shoshone County, Idaho. US Geological Survey Professional Paper, 445. 103 pp.

Gaidies, F., Pattison, D.R.M., de Capitani, C., 2011. Towards a quantitative model of metamorphic nucleation and growth. Contributions to Mineralogy and Petrology 162, 975–993.

Greenwood, H.J., Woodsworth, G.J., Read, P.B., Ghent, E.D., Evenchick, C.A., 1991. Metamorphism. In: Gabrielse, H., Yorath, C.J. (Eds.), Geology of the Cordilleran Orogen in Canada: Geological Survey of Canada, Geology of Canada, 4, pp. 533–570.

Holland, T.J.B., Powell, R., 1998. An internally consistent thermodynamic data set for phases of petrological interest. Journal of Metamorphic Geology 16, 309–344.

Hoy, T., 1989. The age, chemistry, and tectonic setting of the Middle Proterozoic Moyie sills, Purcell Supergroup, southeastern British Columbia. Canadian Journal of Earth Sciences 26, 2305–2317.

Hoy, T., 1993. Geology of the Purcell Supergroup in the Fernie west-half map area, southeastern British Columbia. British Columbia Ministry of Energy, Mines and Petroleum Resources, Geological Surveys Branch, Bulletin, 84. 157 pp.

Hoy, T., Anderson, D., Turner, R., Leitch, C.H.B., 2000. Tectonic, magmatic, and metallogenic history of the early synrift phase of the Purcell Basin, southeastern British Columbia. In: Lydon, J.W., Hoy, T., Slack, J.F., Knapp, M. (Eds.), The geological environment of the Sullivan deposit, British Columbia: Geological Association of Canada, Mineral Deposits Division, Special Publication, 1, pp. 32–60.

Jiang, S.-Y., Palmer, M.R., Slack, J.F., Shaw, D.R., 1998. Paragenesis and chemistry of multistage tourmaline formation in the Sullivan Pb–Zn–Ag deposit, British Columbia. Economic Geology 93, 47–67.

Joncas, I., Beaudoin, G., 2002. The St. Eugene deposit, British Columbia: a metamorphosed Ag–Pb–Zn vein in Proterozoic Belt–Purcell rocks. Economic Geology 97, 11–22.

Kretz, R., 1983. Symbols for rock-forming minerals. American Mineralogist 68, 277–279.

Laberge, J.D., Pattison, D.R.M., 2007. Geology of the western margin of the Grand Forks complex, southern British Columbia: high-grade Cretaceous metamorphism followed by Early Tertiary extension on the Granby fault. Canadian Journal of Earth Sciences 44, 199–228.

Leech, G.B., 1962. Metamorphism and granitic intrusions of Precambrian age in southeastern British Columbia. Geological Survey of Canada Paper 62-13. 8 pp.

Leech, G.B., 1967. In: Wanless, R.K., Stevens, R.D., Lachance, G.R., Edmonds, C.M. (Eds.), Age determinations and geological studies, K–Ar isotopic ages, Report 7: Geological Survey of Canada Paper 66-17, pp. 6–10.

Loomis, T.P., 1986. Metamorphism of metapelites: calculations of equilibrium assemblages and numerical simulations of the crystallization of garnet. Journal of Metamorphic Geology 4, 201–229.

Lydon, J.W., 2000. A synopsis of the current understanding of the geological environment of the Sullivan deposit. In: Lydon, J.W., Hoy, T., Slack, J.F., Knapp, M. (Eds.), The geological environment of the Sullivan deposit, British Columbia: Geological Association of Canada, Mineral Deposits Division, Special Publication, 1, pp. 12–31.

Lydon, J.W., 2007. Geology and metallogeny of the Belt–Purcell Basin. In: Goodfellow, W.D. (Ed.), Mineral deposits of Canada: a synthesis of major deposit-types: Geological Association of Canada, Mineral Deposits Division, Special Publication, 5, pp. 581–607.

Mahar, E.M., Baker, J.M., Powell, R., Holland, T.J.B., Howell, N., 1997. The effect of Mn on mineral stability in metapelites. Journal of Metamorphic Geology 15, 223–238.
McFarlane, C.R.M., Pattison, D.R.M., 2000. Geology of the Matthew Creek metamorphic zone, southeast British Columbia: a window into Middle Proterozoic metamorphism in the Purcell Basin. Canadian Journal of Earth Sciences 37, 1073–1092.
McMechan, M.E., Price, R.A., 1982. Superimposed low-grade metamorphism in the Mount Fisher area, southeastern British Columbia — implications for the East Kootenay orogeny. Canadian Journal of Earth Sciences 19, 476–489.
Obradovich, J.D., Peterman, Z.E., 1968. Geochronology of the belt Series, Montana. Canadian Journal of Earth Sciences 5, 737–747.
Pattison, D.R.M., 1992. Stability of andalusite and sillimanite and the Al_2SiO_5 triple point: constraints from the Ballachulish aureole, Scotland. Journal of Geology 100, 423–446.
Pattison, D.R.M., Tinkham, D.T., 2009. Interplay between equilibrium and kinetics in prograde metamorphism of pelites: an example from the Nelson aureole, British Columbia. Journal of Metamorphic Geology 27, 249–279.
Pattison, D.R.M., Vogl, J.J., 2005. Contrasting sequences of metapelitic mineral-assemblages in the aureole of the tilted Nelson Batholith, British Columbia: implications for phase equilibria and pressure determination in andalusite-sillimanite type settings. The Canadian Mineralogist 43, 51–88.
Pattison, D.R.M., Moynihan, D.P., McFarlane, C.R.M., 2010. Field guide to metamorphism and tectonics in the southern Purcell anticlinorium and Kootenay Arc, southeastern British Columbia (Calgary–Radium–Kimberley–Creston–Riondel–Nelson). Geological Association of Canada field guide series. 151 pp.
Pattison, D.R.M., de Capitani, C., Gaidies, F., 2011. Petrologic consequences of variations in metamorphic reaction affinity. Journal of Metamorphic Geology 29, 953–977.
Powell, W.G., Ghent, E.D., 1996. Low-pressure metamorphism of the mafic volcanic rocks of the Rossland Group, southeastern British Columbia. Canadian Journal of Earth Sciences 33, 1402–1409.
Powell, R., Holland, T.J.B., 2008. On thermobarometry. Journal of Metamorphic Geology 26, 155–179.
Price, R.J., Sears, J.W., 2000. A preliminary palinspastic map of the Mesoproterozoic Belt–Purcell Supergroup, Canada and USA: implications for the tectonic setting and structural evolution of the Purcell Anticlinorium and the Sullivan deposit. In: Lydon, J.W., Hoy, T., Slack, J.F., Knapp, M. (Eds.), The geological environment of the Sullivan deposit, British Columbia: Geological Association of Canada, Mineral Deposits Division, Special Publication, 1, pp. 61–81.
Read, P.B., Woodsworth, G.J., Greenwood, H.J., Ghent, E.D., Evenchick, C.A., 1991. Metamorphic map of the Canadian Cordillera. Geological Survey of Canada Map 1714A, scale 1:2,000,000.
Ross, G., Parrish, R.R., Winston, D., 1992. Provenance and U–Pb geochronology of the Mesoproterozoic Belt Supergroup (northwestern United States): implications of age of deposition and pre-Panthalassa plate reconstructions. Earth and Planetary Science Letters 113, 57–76.
Schandl, E.S., Davis, D.W., 2000. Geochronology of the Sullivan deposit: U–Pb and Pb–Pb ages of zircons and titanites. In: Lydon, J.W., Hoy, T., Slack, J.F., Knapp, M. (Eds.), The geological environment of the Sullivan deposit, British Columbia: Geological Association of Canada, Mineral Deposits Division, Special Publication, 1, pp. 127–135.
Schandl, E.S., Davis, D.W., Gorton, M.P., 1993. The Pb-Pb age of metamorphic titanite in the chlorite–pyrite altered footwall of the Sullivan Zn–Pb SEDEX deposit, British Columbia, and its relationship to the ore. Geological Association of Canada/Mineralogical Association of Canada, Program with Abstracts 18, A93.
Seitz, J.D., 2009. Metamorphism of alteration zones surrounding the St. Eugene Mine, SE British Columbia. Unpublished B.Sc. thesis, University of Calgary, 52 pp.
Shaw, D.M., 1956. Geochemistry of pelitic rocks. Part III: major elements and general geochemistry. Geological Society of America Bulletin 67, 919–934.
Slack, J.F., Shaw, D.R., Leitch, C.H.B., Turner, R.J.W., 2000. Tourmalinites and coticules from the Sullivan Pb–Zn–Ag deposit and vicinity, British Columbia: geology, geochemistry and genesis. In: Lydon, J.W., Hoy, T., Slack, J.F., Knapp, M. (Eds.), The geological environment of the Sullivan deposit, British Columbia: Geological Association of Canada, Mineral Deposits Division, Special Publication, 1, pp. 736–767.
Spear, F.S., 1988. Metamorphic fractional crystalization and internal metasomatism by diffusional homogenization of zoned garnets. Contributions to Mineralogy and Petrology 99, 507–517.
Spear, F.S., Cheney, J.T., 1989. A petrogenetic grid for pelitic schists in the system SiO2–Al2O3–FeO–MgO–K2O–H2O. Contributions to Mineralogy and Petrology 101, 149–164.
Symmes, G.H., Ferry, J.M., 1992. The effect of whole-rock MnO content on the stability of garnet in pelitic schists during metamorphism. Journal of Metamorphic Geology 10, 221–237.
Thompson, J.B., 1957. The graphical analysis of mineral assemblages in pelitic schists. American Mineralogist 42, 842–858.
Tinkham, D.K., Ghent, E.D., 2005. Estimating P–T conditions of garnet growth with isochemical phase diagram sections and the problem of effective bulk-composition. The Canadian Mineralogist 43, 35–50.
Tinkham, D.K., Zuluaga, C.A., Stowell, H.H., 2001. Metapelite phase equilibria modeling in MnNCKFMASH: the effect of variable Al_2O_3 and MgO/(MgO+FeO) on mineral stability. Mineralogical Society of America: Geological Materials Research 3, 1–42.
Turner, R.J.W., Leitch, C.H.B., Hoy, T., Ransom, P.W., Hagen, A., Delaney, G.D., 2000. Sullivan graben system: district-scale setting of the Sullivan deposit. In: Lydon, J.W., Hoy, T., Slack, J.F., Knapp, M. (Eds.), The geological environment of the Sullivan deposit, British Columbia: Geological Association of Canada, Mineral Deposits Division, Special Publication, 1, pp. 370–407.
Waters, D.J., Lovegrove, D.P., 2002. Assessing the extent of disequilibrium and overstepping of prograde metamorphic reactions in metapelites from the Bushveld Complex aureole, South Africa. Journal of Metamorphic Geology 20, 135–149.
Wei, C.J., Powell, R., Clarke, G.L., 2004. Calculated phase equilibria for low- and medium-pressure metapelites in the KFMASH and KMnFMASH systems. Journal of Metamorphic Geology 22, 495–508.
White, W.H., 1959. Cordilleran tectonics in British Columbia. American Association of Petroleum Geologists Bulletin 43, 60–100.
Zeh, A., Holness, M.B., 2003. The effect of reaction overstep on garnet microtextures in metapelitic rocks of the Ilesha Schist Belt, SW Nigeria. Journal of Petrology 44, 967–994.